WIDE-ANGLE ASTROMETRY WITH THE MARK III STELLAR INTERFEROMETER

M. Shao,[a] M. M. Colavita,[a] and B. E. Hines[b]
Jet Propulsion Laboratory, 4800 Oak Grove Drive, Pasadena, California 91109

J. L. Hershey, J. A. Hughes, D. J. Hutter, and G. H. Kaplan
U. S. Naval Observatory, Washington, DC 20392-5100

K. J. Johnston,[c] D. Mozurkewich,[c] and R. S. Simon[c]
Center for Advanced Space Sensing, Naval Research Laboratory, Washington, DC 20375

X. P. Pan[a]
Department of Astronomy, California Institute of Technology, Pasadena, California 91125
Received 29 June 1990; revised 2 August 1990

ABSTRACT

Astrometric measurements made with the Mark III stellar interferometer on five nights in August–September 1988 yielded average formal 1σ errors for 12 FK5 stars of 6 mas in declination and 10 mas in right ascension. This improvement in precision over previously reported measurements with this instrument made in 1986 is attributable to several factors: a second 12 m baseline; oriented E–S, was added to the instrument to improve the determination of right ascension; two-color analysis was included in the data-reduction process, along with a new central-fringe identification algorithm using three spectral channels, in order to reduce atmospheric errors; thermal control was greatly improved; and changes were made to observational procedures and hardware to monitor variations in the delay offset due to residual thermal drifts. Approximately half of the new positions are within 50 mas of their FK5 positions. However, an extended series of measurements are needed to ascertain the accuracy that can be achieved by interferometry.

I. INTRODUCTION

The Mark III stellar interferometer on Mount Wilson, California, after a 2.7 yr construction program, began observations in September 1986 (Shao *et al.* 1988). A set of preliminary astrometric measurements using a N–S baseline in November 1986 demonstrated 20 milliarcsec (mas) precision in declination (Mozurkewich *et al.* 1988). Since that time, several improvements have been made to the instrument, the observing procedure, and the data reduction process to improve the quality of the astrometric observations.

A schematic of the Mark III interferometer as used for astrometry is given in Fig. 1; a detailed description of the instrument is given by Shao *et al.* (1988). The three siderostats in the figure are housed in octagonal-shaped weather enclosures; two additional siderostats (not shown) are used for variable-baseline imaging. The north and south siderostats form a 12 m N–S baseline, while the east and south siderostats form a 12 m E–S baseline. Only one baseline can be used at a time. These siderostats are mounted on 2 ft $\times$ 4 ft-wide piers that rise 4 ft above ground level and go 4–8 ft below ground level to bedrock. The piers are not directly connected to the concrete pads that support the weather enclosures. The piers and their weather enclosures are insulated with 2 in. of foam, and are air conditioned during the day to approximately the nighttime temperature.

Light from the siderostats is directed into a temperature-controlled beam-combining building, and optical path delay is introduced with active laser-monitored optical delay lines. The stellar fringe is detected coherently, both in a wideband channel near 0.7 μm, which is used to generate an error signal for the stellar fringe tracker, as well as in narrowband channels at 0.5 and 0.8 μm. An autoguider maintains wave front parallelism between the beams from the two siderostats.

The instrument is highly automated. At the beginning of the night, a star list is loaded into the sequencing computer. This list is cycled through repeatedly, with stars below the instrument's zenith limit automatically skipped. Siderostat and delay-line slewing, acquisition, tracking, and data recording are all automated, normally requiring no operator intervention. Additionally, automatic delay-offset calibration, discussed below, is performed once per cycle. Each star is typically observed for 90 s (a "scan") during each cycle of the star list, for a total of 100–200 scans per night. For some nights, alternate baselines were used for each cycle; on other nights, the same baseline was used all night.

II. WIDE-ANGLE ASTROMETRY WITH OPTICAL INTERFEROMETERS

Optical astrometry with long-baseline interferometers is very similar to VLBI astrometry. The basic astrometric equation is

$$x = \hat{\mathbf{s}} \cdot \overline{\mathbf{B}} + C, \tag{1}$$

where the delay x is the position of the central white-light fringe, $\hat{\mathbf{s}}$ is the unit vector to the star, $\overline{\mathbf{B}}$ is the baseline vector, and C is the delay offset, which depends on the details of the interferometer optical path and on the zero point of the laser metrology system.

The optical delay lines, located in two 5-m-long vacuum
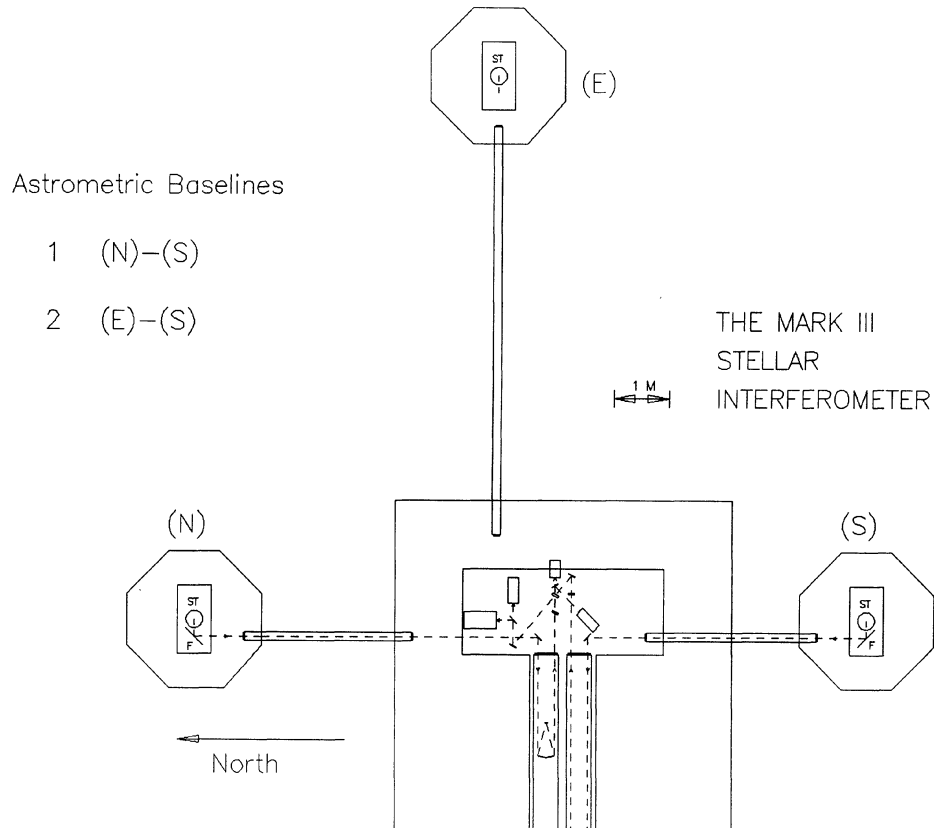
0004-6256/90/051701-11$00.90

FIG. 1. Schematic of the Mark III interferometer.

chambers, are moved to equalize the path lengths from the star to the beam combiner via the two arms of the interferometer. The positions of the delay lines are measured with a laser interferometer with 5 nm resolution at a 1 kHz rate. Figure 2 shows a plot of delay versus time for one night of observation. These data were taken alternately with the N–S and E–S baselines. The curves displayed are all parts of 24 hr sinusoids, one for each star observed on each baseline.

We report here observations and analysis of a wide-angle set of 12 stars observed over five nights in August and September 1988. The analysis procedure is similar to that described by Mozurkewich *et al.* (1988), with differences attributable to the addition of two-color processing and delay-offset calibration. Corrections to the apparent star positions due to precession, nutation, etc., were performed with the U. S. Naval Observatory astrometry subroutine package NOVAS, which conforms to the IAU convention for coordinate transformations (Kaplan *et al.* 1989).

The raw data recorded by the instrument consists of 4 ms samples of the stellar fringe in three spectral channels: a wide red channel at 0.7 μm ($\Delta\lambda \simeq 300$ nm), a narrow red channel at 0.8 μm ($\Delta\lambda = 25$ nm), and a narrow blue channel at 0.5 μm ($\Delta\lambda = 40$ nm). The delay-line position, along with calibration data, is also recorded. The data are processed to give the average delays over 1 s intervals, incorporating two-color processing and delay offset calibration as discussed in the next two sections. These averaged delays are used with an *a priori* model of the instrument geometry to calculate the residual delays, and to determine the partial derivatives of the

delays with respect to the quantities of interest. The residuals are then averaged to a scan, i.e., the observation time per star per cycle of the star list, which is approximately 90 s for these data. The residuals and partial derivatives are used in a least-squares program to solve for the quantities of interest. (It might be noted that with an interferometer that equalizes path length in vacuum, there is no first-order astronomical refraction. For one-color observations, a simple atmospheric model is used to remove the small second-order refraction (Mozurkewich *et al.* 1988); for two-color observations, this effect is automatically corrected, and no modeling is necessary.

The reference set consisted of 12 stars with good hour-angle coverage that were repeatedly observed over the five nights. These stars covered a range of $\sim 90°$ in right ascension and $\sim 45°$ in declination, as shown in Fig. 3. The star positions were determined relative to a mean FK5 position using the following procedure. Assuming the FK5 positions for the stars, the interferometer baselines were determined for each night. Using these baselines, updated star positions were determined using all five nights of data. Using these updated star positions, a new set of baselines was determined. This last set of baselines was used to derive the final star positions. Clearly, since the original FK5 positions are used to derive the interferometer baselines, these solutions are susceptible to systematic biases in the FK5. However, this procedure is useful for demonstrating the precision of the interferometric measurements.

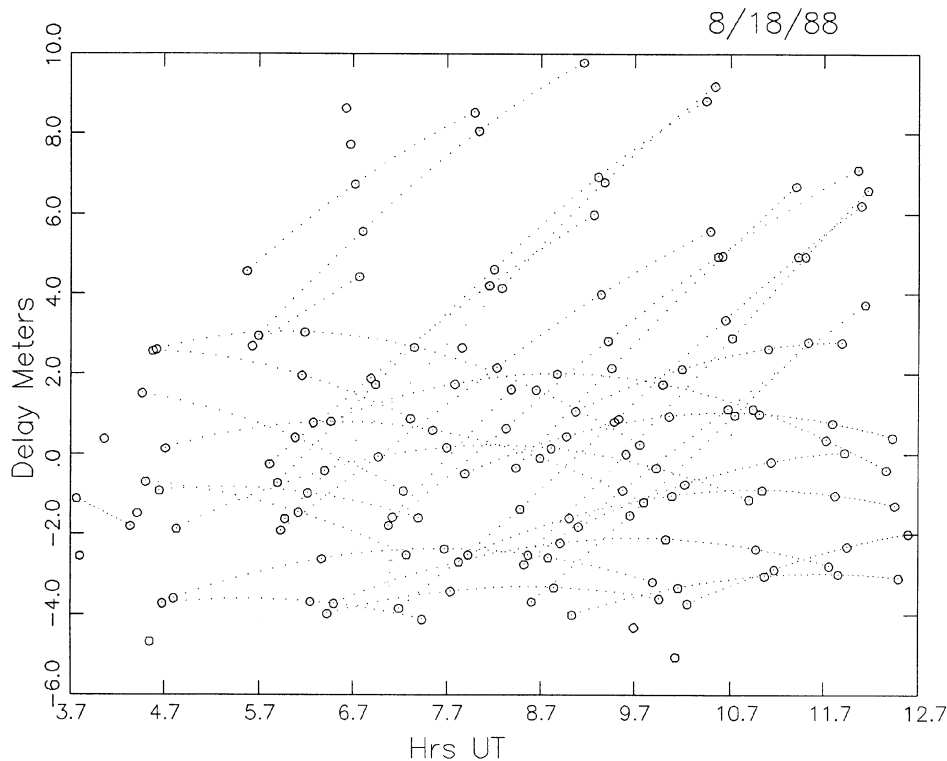The addition of two-color delay corrections and delay-

FIG. 2. Delays for 183 scans of 21 stars with two baselines measured on 18 August 1988.

offset calibration is a departure from the processing used previously (Mozurkewich *et al.* 1988), and is discussed in detail below.

III. TWO-COLOR DELAY CORRECTION

a) Two-Color Astrometry

The turbulent atmosphere is the fundamental limitation to high-accuracy astrometry from the ground. Atmospheric turbulence generates refractive-index variations which cause fluctuations in the apparent positions of stars. Because much of the energy in these fluctuations corresponds to very low spatial frequencies, these fluctuations introduce position errors which decrease very slowly with integration time. One means to reduce these errors is to switch rapidly among stars in order to reject the lowest frequency errors. Another is to reduce the atmospheric error directly. The two-color method exploits the dispersion of the atmosphere in order to estimate simultaneously the instantaneous stellar position as well as the instantaneous atmospheric error. The two-color estimate x_{2C} of a delay can be written:

$$x_{2C} = x_R - D(x_B - x_R),\qquad(2)$$

where x_R and x_B are the delays measured in the red and blue channels, and D is the dry-air dispersion: $D = [n(\lambda_R) - 1]/[n(\lambda_B) - n(\lambda_R)]$, where $n(\lambda)$ is refractive index. For red and blue wavelengths of 0.7 and 0.5 μm, the dispersion D is equal to 87.1. The second term in the equation above can be interpreted as the instantaneous atmospheric error, so that, in principle, the two-color estimate is a measure of the true delay.

A detailed analysis of the two-color method, as well as a limited set of experimental data, has been presented previously (Colavita *et al.* 1987). The main conclusion of the

theoretical analysis was that the degree of improvement in accuracy possible with the two-color method is limited by turbulent water-vapor fluctuations. At optical wavelengths, the main contribution to atmospheric seeing is temperature microfluctuations; these are corrected by the two-color method. The residual after correction is the water-vapor contribution, which will have the same statistics as the temperature microfluctuations, with an estimated amplitude 5 to 10 times smaller. Application of the two-color method to stellar data in that work demonstrated a factor of 5 reduction in the amplitude of the delay fluctuations. Additional atmospheric errors affecting two-color measurements were also investigated. Most of these were shown to introduce white-noise errors which decreased rapidly with integration time. Photon statistics in the measurement of fringe phase also introduces a white-noise error which rapidly integrates out. The most important systematic error was expected to be caused by residual instrumental dispersion caused by mismatches in the composition of optical windows in the system. This error is minimized in the present setup by using a narrow bandwidth for the blue channel, where material dispersion is the highest.

b) Central Fringe Identification

Data processing for two-color measurements is similar to that presented previously (Colavita *et al.* 1987), but with several improvements. The wideband red channel, which is used in real time for fringe tracking, is used as a phase reference in order to synthesize a longer coherence time for the narrowband channels. The phase-referenced coherence time for the narrowband channels was usually 200 ms, consisting of 50 4 ms raw data points. In the present configuration, variable binning electronics correct for systematic errors
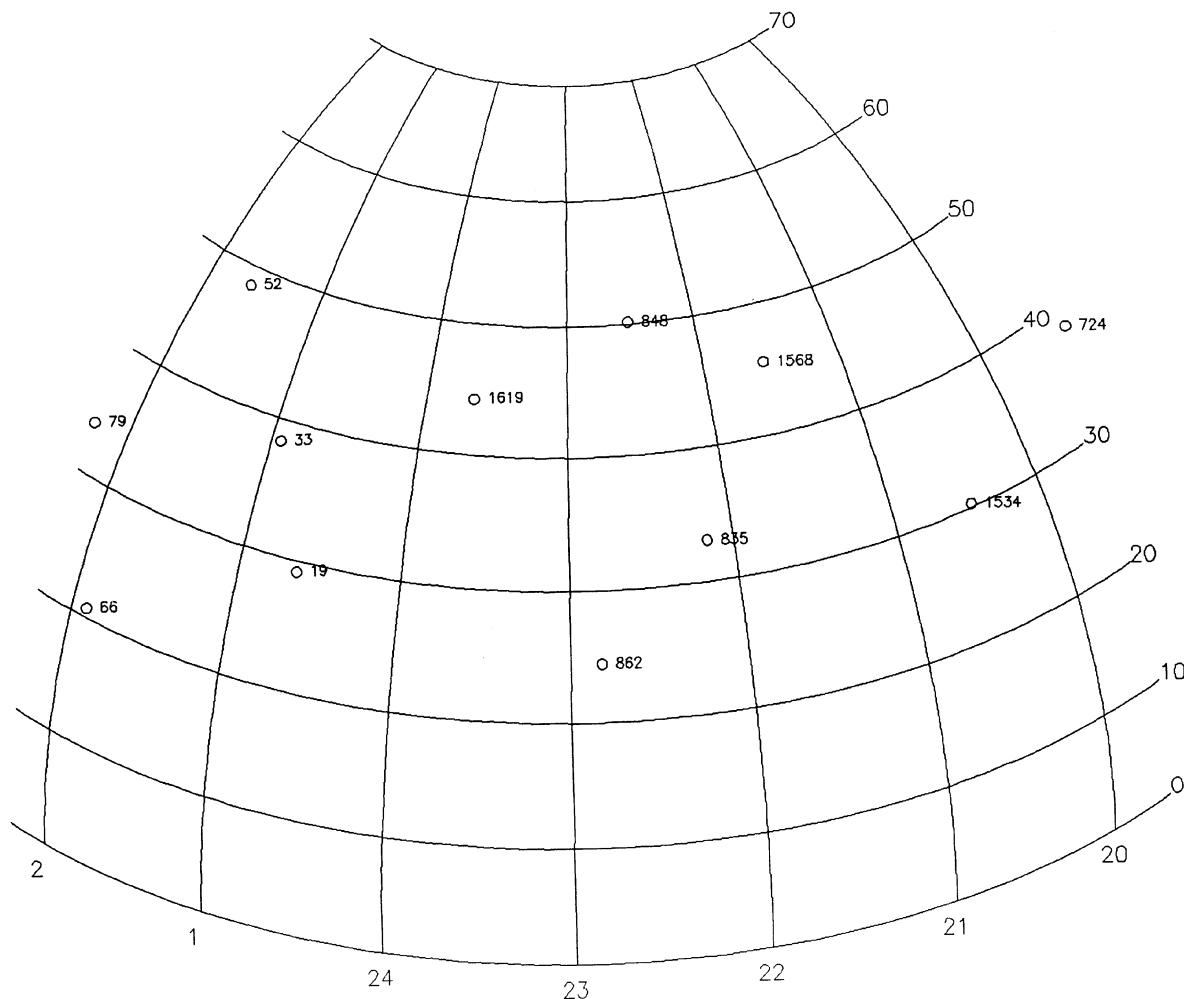
FIG. 3. Sky coverage of the test set.

caused by differences between the length of the path-length modulation stroke and the desired wavelength, by changing the amount of deadtime at the ends of the modulation.

In the practical application of the two-color method, the most important step is reliable central fringe identification. All phases must be referenced to the central white-light fringe. In real time, this is accomplished with a centering algorithm which uses the mean fringe visibility to maintain the zero point of the tracker on the central (zero-order) fringe, in conjunction with a phase-unwrapping algorithm which keeps track of the integer fringe count. Occasional undetected unwrapping errors are usually unimportant for one-color astrometry. However, for two-color astrometry, unwrapping errors introduce large errors because of the magnitude of the dispersion constant D in Eq. (2).

Three discriminants are used to edit the two-color data: (A) the primary two-color position, given above, using the narrowband blue ($\lambda_B = 0.5 \, \mu$m) and wideband red ($\lambda_R = 0.7 \, \mu$m) channels, for which $D = 87.1$, (B) a secondary two-color position using the wideband red (0.7 μm) and the narrowband red (0.8 μm) channels, for which $D = 364$, and (C) the fringe visibility in the wideband red channel.

(In addition, there is a minimum acceptable signal-to-noise ratio for each of the three channels.) The simplest two-color selection algorithm is just to window on the primary two-color position (A). In theory, assuming perfect two-color correction of the atmospheric error, the two-color residual should be exactly zero when the track point is on the central fringe, and equal to $nD(\lambda_R - \lambda_B)$ when the track point is off by n fringes. However, the difference $n(\lambda_R - \lambda_B)$ is actually taken modulo λ_B, so that with $\lambda_R = 0.7 \, \mu$m and $\lambda_B = 0.5 \, \mu$m, track-point errors greater than one fringe wrap around to near zero. Thus, the secondary two-color position, which uses more closely spaced wavelengths, is useful for detecting multiple-fringe errors. The fringe visibility is also used as a discriminant to reject data whose track point is different from zero. However, because of a slight residual dispersion in the instrument which shifts the peak of the fringe visibility away from zero phase, the fringe visibility is most useful for rejecting data for which the track-point error is two fringes or larger.

Figures 4–6 give plots of the three discriminants (A), (B), and (C) for a scan from this dataset which exhibited significant fringe hopping. Each point in the figures repre-
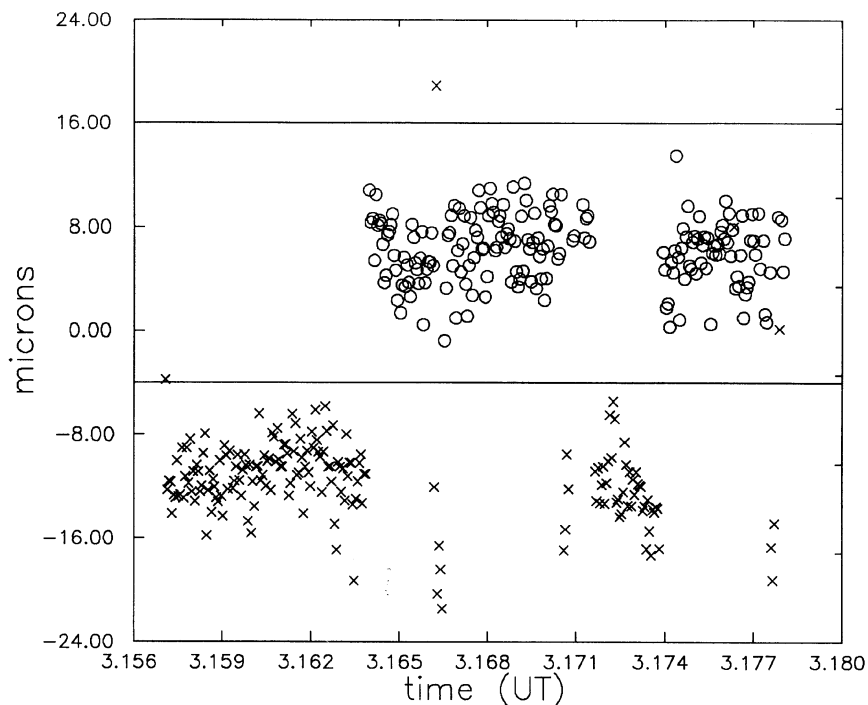
FIG. 4. Two-color discriminant A [primary two-color residual using wideband red (0.7 μm) and narrowband blue (0.5 μm)] for one scan. Each point corresponds to 200 ms of data; points rejected by any of the three discriminants are indicated by ×.

sents 200 ms of data. Three fringes are visible in each figure. In Fig. 4, a plot of the primary two-color position, the central fringe has a mean residual of ∼6 μm (the zero point of the figure is arbitrary), the − first-order fringe is at ∼ − 13 μm, and the + first-order fringe wraps around to ∼ − 18 μm. That the two first-order fringes are distinct is made clear in Fig. 5, a plot of the secondary two-color position divided

by the dispersion *D*, where the smaller separation between the wavelengths prevents the position from wrapping, eliminating the ambiguity in Fig. 4. Figure 6 shows the wideband fringe visibility. While the fringe visibility is significantly lower for the + first-order fringe than for the central fringe, an asymmetry in the fringe envelope causes the central fringe and − first-order fringe to have nearly the same visibility.
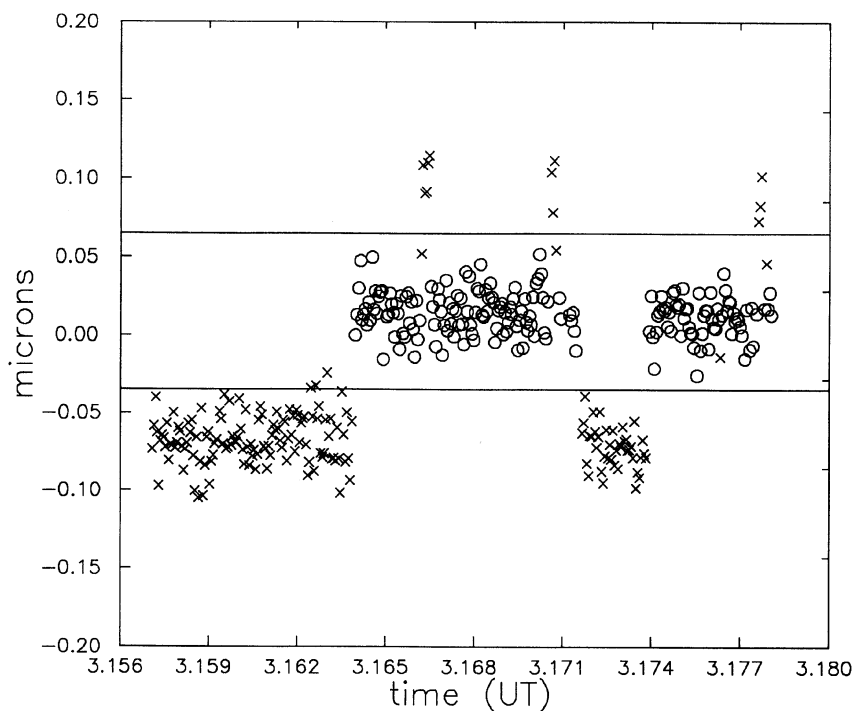

FIG. 5. Two-color discriminant B [secondary two-color residual using wideband red (0.7 μm) and narrowband red (0.8 μm)] for one scan. Each point corresponds to 200 ms of data; points rejected by any of the three discriminants are indicated by ×.

FIG. 6. Two-color discriminant C [fringe visibility in wideband red $(0.7 \mu m)$] for one scan. Each point corresponds to 200 ms of data; points rejected by any of the three discriminant are indicated by $\times$.

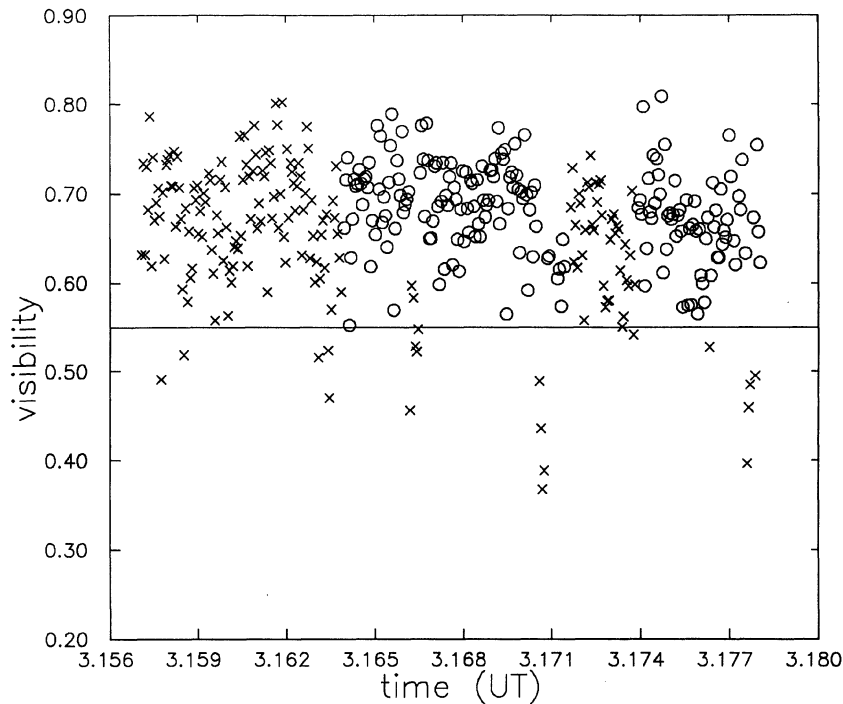However, by using all three discriminants, unambiguous determination of the central fringe is possible. For reference, Fig. 7 shows the one-color fringe position for the same scan. The 20 μm peak-to-peak motion exhibits significant energy at low spatial scales, as expected. The smaller low-spatial-scale fluctuations in the two-color position of Fig. 4 are partially masked by a white-noise term on these 200 ms timescales.

After the central-fringe identification process, a simple median filter was used to remove any remaining outliers. In order to provide a fair comparison between one- and two-color positions, the one-color data were edited in precisely the same manner as the two-color data. However, differences between the statistics of the edited and unedited one-color data were very small. After median filtering, the data were averaged to one scan, and processed as discussed above.
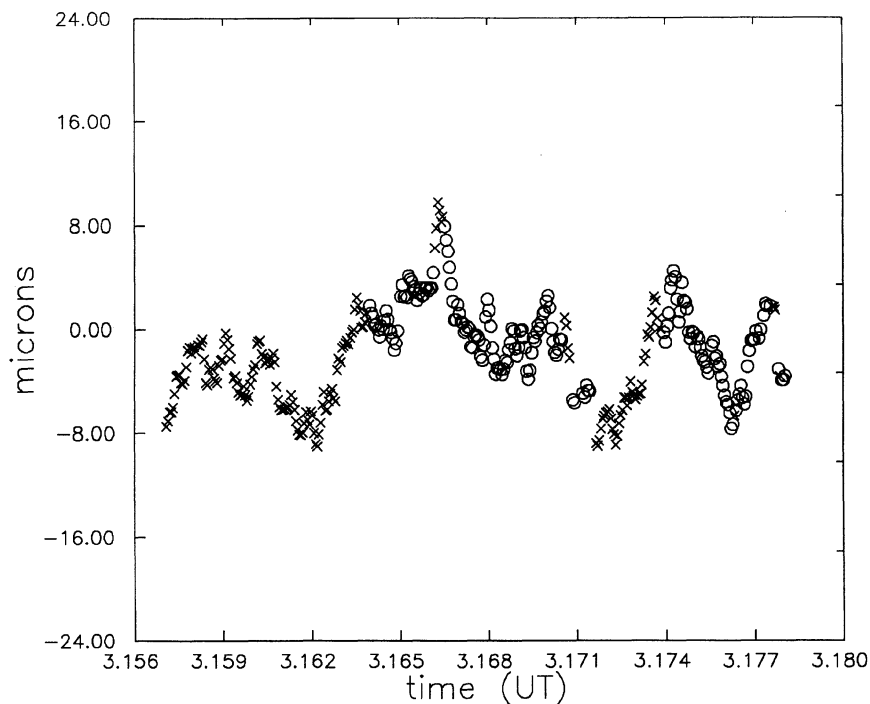

FIG. 7. One-color fringe position for one scan. Each point corresponds to 200 ms of data.
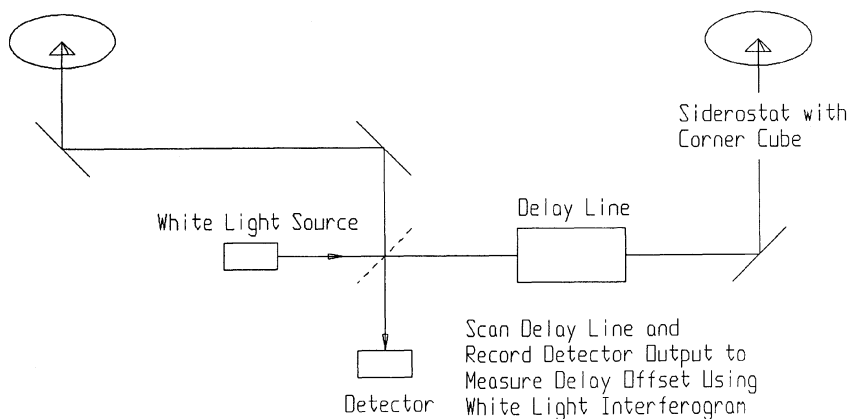
FIG. 8. Schematic of delay-offset calibration optics.

IV. DELAY-OFFSET CALIBRATION

Equation (1) has two terms associated with the instrument: the baseline vector $\overline{\mathbf{B}}$ and the delay offset C. The analysis so far assumes that $\overline{\mathbf{B}}$ and C are constant for one night's observation. Unfortunately, thermal effects cause both the baseline vector and delay offset to drift during the night. In the previous paper (Mozurkewich *et al.* 1988), a linearly varying baseline and delay offset were explicitly determined. In the present case, in order to remove one component of this error, the instrument was modified to measure the thermal changes to the delay offset throughout the night.

The delay offset, i.e., the difference between the optical path lengths from the beam combiner to each of the two siderostats with the delay lines at their nominal zero positions, is measured with an internal white-light interferometer as shown schematically in Fig. 8. Light from an internal white-light source is directed toward the main interferometer beam splitter and propagates backwards through the interferometer optics to corner cubes located on the siderostats. The retroreflected light then reenters the interferometer, interferes at the beam splitter, and is detected by the same PMTs used for star light. The delay line is then scanned under laser control and an interferogram recorded.

Corner cubes attached to the siderostat mirrors were used instead of the mirror surfaces themselves as the retroreflectors for the white light in order to reduce the requirements on the accuracy of mirror tilt needed to detect fringes. Because of local turbulence, the white-light fringe was scanned four to eight times and the positions of the central fringe averaged. A low-order polynomial was used to interpolate the delay offset for each scan of stellar data. The results of this interpolation were then used to correct the raw delay as discussed in Sec. II.

The original observing strategy was to observe a set of stars alternately on the N–S and E–S baselines. Switching baselines was accomplished with a slide-in mirror controlled by the sequencing computer. The delay-offset data shows that occasionally the slide-in mirror would not repeat to its design accuracy. As a result, for the last two nights of observations reported here, only one baseline was used each night. These two nights, one with each baseline, were then combined and treated as a single night in order to solve for stellar positions. This change in the observing strategy ensured that the data would always be usable, though of lower accuracy, without the delay-offset calibration.

V. RESULTS AND DISCUSSION

An experiment summary is presented in Table I. Of the stars that were observed over the five nights, 12 were chosen that had good hour-angle coverage. However, in solving for baselines, one star (FK5 724) was excluded, as it was observed on only four of the five nights. The nights, baselines, and scans per night for these stars are given in Table I. Each star had approximately 50 total scans over the observation period, for a total of 588 for the entire set. (This is a subset of the 859 total observations over that period.)

Positions were determined for these stars using the least-squares method previously discussed using one-color, one-

TABLE I. Measurement summary.

Date (UT)	N–S baseline	E–S baseline
14 August 1988	68 scans spanning 7.5 hr	59 scans spanning 7 hr
15 August 1988	70 scans spanning 9 hr	59 scans spanning 8 hr
18 August 1988	57 scans spanning 9 hr	51 scans spanning 7 hr
15 September 1988	106 scans spanning 10 hr	
16 September 1988		118 scans spanning 10 hr

star list(FK5): 19, 33, 52, 66, 79, 724, 835, 848, 862, 1534, 1568, 1619.
star list(FK5) for baseline solution: as above, but exclude 724.

color with delay-offset calibration, and two-color with delay-offset calibration. A summary of the 1σ formal errors for these three cases is given in Table II, along with the rms residuals to the raw delays. The two-color positions relative to the FK5 positions, along with the 1σ formal errors, are tabulated in Table III and are plotted in Fig. 9. The box in the center of Fig. 9 represents the approximate 50 mas accuracy of the FK5 positions at epoch 1988. The crosses represent the offset of the Mark III measurements from the FK5 positions, and the size of the crosses represents the formal errors of those measurements. Approximately half of the Mark III positions are within the FK5 error box, showing that for this set, the agreement between our measurements and the FK5 is as expected.*†

The final results are an average formal error of the two-color measurements using the delay-offset calibration of 5.6 mas in declination and 9.2 mas in right ascension. These are a factor of ~2.1 smaller than the uncalibrated one-color measurements, as shown in Table II. The formal error in declination is smaller than that in right ascension because of the geometry of the two baselines used for astrometry. Each baseline has an error ellipse that is much narrower in the direction perpendicular to the baseline. Thus, the combination of a N–S and an E–S baseline results in an error ellipse that is smaller in the declination direction than in the right ascension direction; with orthogonal baselines, the errors would be expected to be more nearly equal.

To check on the self-consistency of the data, stellar positions were also determined for each night of data alone, using the previously determined baselines for each night. The rms differences between these solutions and the global solution were approximately 1.8 times the formal error for the global solution, close to the expected factor of $\sqrt{4}$.

In the previous paper (Mozurkewich *et al.* 1988), 20 mas precision in the measurement of declination, and 75 mas precision in right ascension was demonstrated using seven nights of one-color data obtained with a single 12 m N–S baseline. The present results represent a total improvement of a factor of 3.6 in declination and 8.1 in right ascension. The significant improvement in the right ascension precision over the results from 1986 is attributable primarily to the inclusion of the E–S baseline, whose E–W component greatly increases the accuracy of right ascension measurements. However, the declination precision is also considerably better in the present case, even without the two-color correction. This is due in part to improvements in instrumental stability brought about by monitoring the delay offset using the internal white-light source, and by improved thermal control, including air conditioning of the siderostat buildings during the day in order to eliminate thermal drifts at the beginning of the night. In addition, observations of delay-offset drifts of the shape shown in Fig. 10 led us to abandon

the use of a linearly varying baseline model for each night. Part of the gain over the previous one-color measurements is also attributable to somewhat better seeing during the period of these observations: the seeing for these measurements was better than 0.5 arcsec.

The effectiveness of the delay-offset calibration is illustrated in Figs. 10 and 11. Figure 10 shows the delay-offset drift versus time on 16 September 1988. The positive excursions near 6 and 10 hr are correlated with sudden changes in the outside temperature. Figure 11 is a plot of the delay residuals on 16 September 1988 using the two-color correction, but without the constant-term calibration. These data are smoothed by an 11-point running average. Comparison of the two figures shows that the monitored delay-offset variations are highly correlated with the uncalibrated delay residuals. The effectiveness of the delay-offset calibration is somewhat masked in the results of Table II by the one-color atmospheric noise. As the instrument geometry consists of four parameters, it is somewhat surprising that such a large fraction of the residual instrument error is correlated with just the delay offset.

The application of the two-color method is also important in order to obtain the present high precision, providing an improvement over the calibrated one-color formal errors of a factor of 1.7. While the precision of the one-color measurements appears to be limited by the atmosphere, we believe the two-color measurements are limited by thermal drifts of the instrument not monitored by the laser system or the white-light constant-term calibration; in particular, the orientation of the baseline vector relative to the rotation axis of the Earth is very difficult to monitor.

One measure of the atmospheric fluctuations which should be independent of any instrumental errors is the rms of the points within the individual scans. Table IV gives the median intrascan standard deviations for the five nights using one- and two-color processing for the data binned to ~0.8 s and ~15 s segments.‡ In the previous paper (Mozurkewich *et al.* 1988) the 1 s intrascan rms was used as a measure of the data quality. However, this timescale is too short to eliminate the white-noise component of the two-color position, which rapidly integrates out: the ratio of the mean one-color to two-color intrascan rms improves from 2.5 to 3.6 when increasing the segment size from 0.8 to 15 s. Assuming a similar power law for the residual one- and two-color errors, which is predicted by theory, and neglecting any residual white-noise component in the two-color rms, the numbers in the table suggest that a mean reduction in the atmospheric error of ~3.6 should be achievable. Thus, if the atmosphere were the only limiting factor, one would expect a commensurate reduction in the formal errors, greater than the 1.7 achieved. So it appears that the two-color astrometric precision is limited by instrumental effects. Previous experiments with the two-color method (Colavita *et al.* 1987) have shown that a factor of 5 improvement should be possible on good nights. Thus, the data presented in the table, showing factors of 2.5–8.0 improvement, are consistent with these earlier observations.

---

*β Ari is a spectroscopic double that has recently been resolved by the Mark III interferometer (Pan *et al.* 1990), yielding a semimajor axis of 36.1 mas. Its duplicity was ignored in calculating its *a priori* position.

†Similar agreement is obtained between the Mark III results and preliminary star positions determined with the 6 in. transit circle in Washington, DC, from September 1985 to March 1989, as part of a program to observe the International Reference Stars. Excluding FK5 star 835, the rms differences between the Mark III results and the Washington transit circle results are 44 mas in right ascension and 37 mas in declination, while the rms differences between the Mark III results and the FK5 positions are 65 mas in right ascension and 42 mas in declination.

---

‡Because of occasional losses of fringe tracking, the individual 200 ms points in the 90 s scans are not all contiguous or of the same number. For calculating the 15 s quantities, the 200 ms data were binned in groups of size 2^n, where n is some integer, so that the standard deviation within the 90 s scan was computed from between four and seven samples.

TABLE II. Error summary.

Mode	Average formal (1σ) errors		Residuals	
	right ascension	declination	N–S baseline	E–S baseline
one-color	19.8 mas	12.1 mas	2.85 μm	3.85 μm
one-color with delay-offset calibration	15.6 mas	9.5 mas	2.42 μm	2.89 μm
two-color with delay-offset calibration	9.2 mas	5.6 mas	1.47 μm	1.65 μm

TABLE III. Two-color positions relative to FK5 with 1σ formal errors.

FK5 no.	Scans	Right ascension offset (mas)	Declination offset (mas)
724	24	+ 90.2 ± 15.3	+ 54.3 ± 7.1
1534	46	+ 35.4 ± 8.7	− 8.8 ± 5.2
1568	49	+ 10.9 ± 10.5	+ 27.8 ± 5.6
835	60	+ 36.2 ± 7.9	+ 69.4 ± 4.9
848	50	+ 99.1 ± 10.9	− 42.5 ± 5.9
862	58	− 78.2 ± 7.1	− 32.9 ± 5.1
1619	54	− 86.3 ± 10.1	− 2.7 ± 5.3
19	51	− 28.7 ± 8.2	+ 0.6 ± 5.4
33	57	− 24.1 ± 8.8	+ 17.3 ± 5.3
52	44	− 30.6 ± 11.7	+ 25.2 ± 6.3
66	46	+ 103.9 ± 8.0	+ 7.1 ± 6.3
79	49	− 6.8 ± 8.9	− 85.3 ± 6.3
total scans 588		mean error 9.2	mean error 5.6

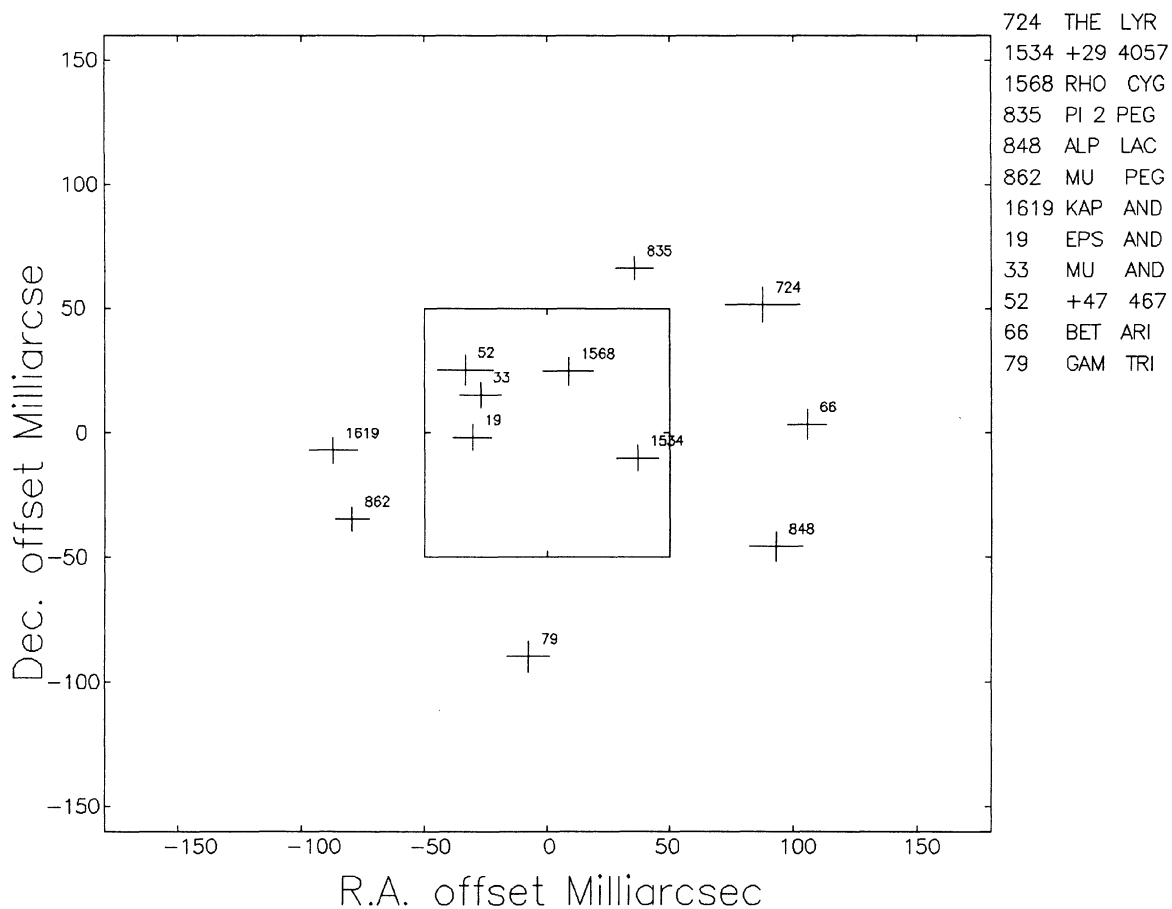| 724 | THE | LYR |
1534	+29	4057
1568	RHO	CYG
835	PI 2	PEG
848	ALP	LAC
862	MU	PEG
1619	KAP	AND
19	EPS	AND
33	MU	AND
52	+47	467
66	BET	ARI
79	GAM	TRI

FIG. 9. New star positions using two-color correction and delay-offset calibration. The 1σ formal error bars for each star are indicated. All positions are relative to the FK5 positions.
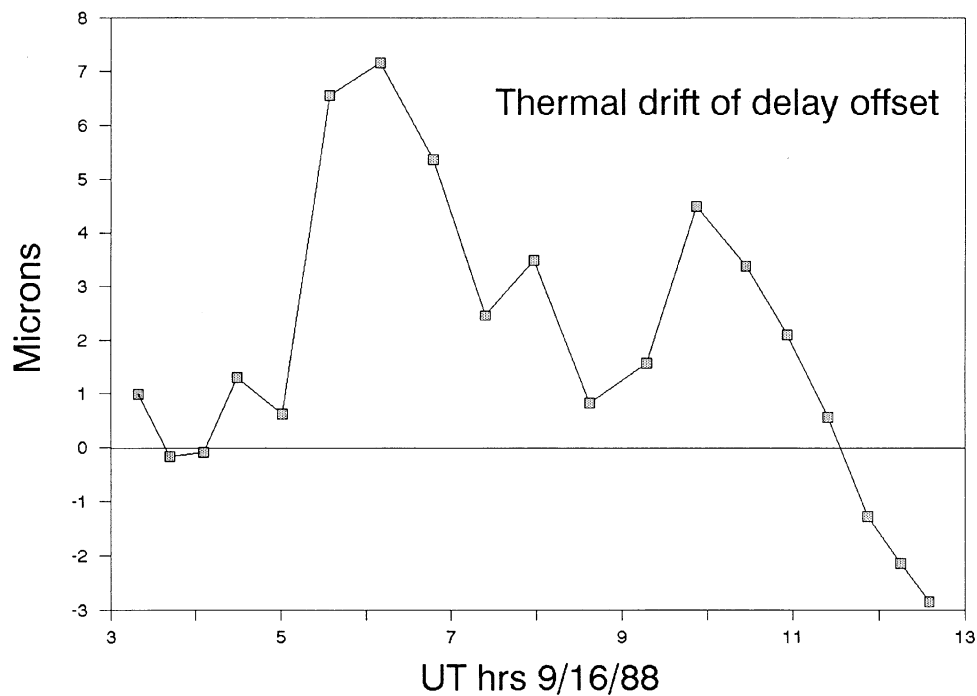
FIG. 10. Delay offset vs time for observations on 16 September 1988.
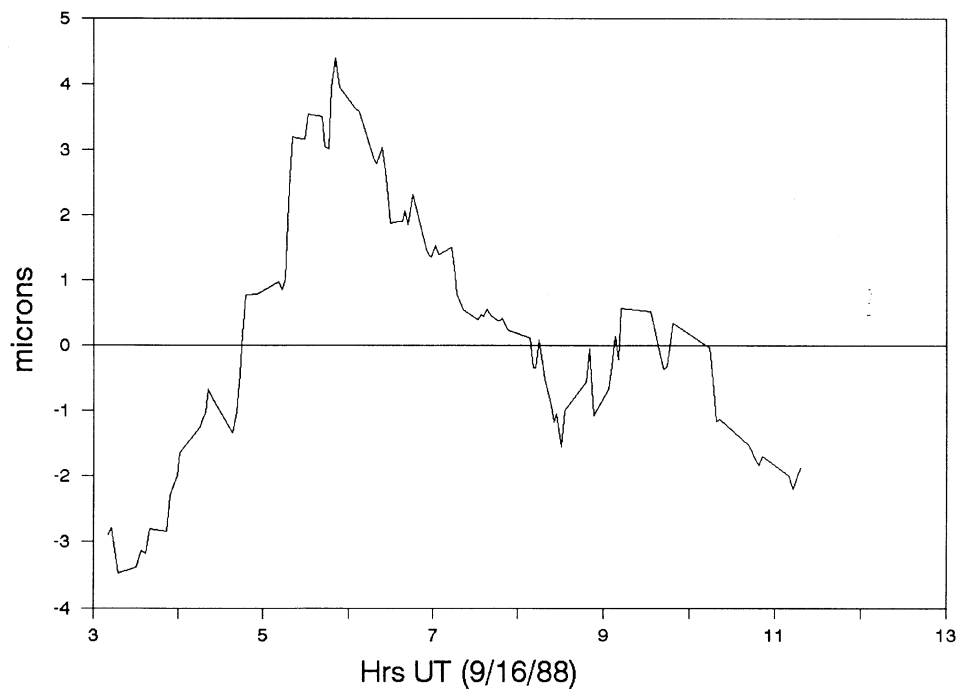

FIG. 11. Delay residuals vs time for observations on 16 September 1988 using two-color correction, but excluding delay-offset calibration. The residuals are smoothed by an 11-point running average.

TABLE IV. Median intrascan fluctuations (rms).

Date (UT)	One-color		Two-color	
	0.8 s points	15 s points	0.8 s points	15 s points
14 August 1988	2.72 μm	1.61 μm	0.59 μm	0.20 μm
15 August 1988	2.72 μm	1.66 μm	0.79 μm	0.33 μm
18 August 1988	2.90 μm	1.77 μm	1.64 μm	0.71 μm
15 September 1988	2.66 μm	1.72 μm	1.09 μm	0.47 μm
16 September 1988	2.98 μm	1.87 μm	1.41 μm	0.70 μm
	mean	mean	mean	mean
	2.80 μm	1.73 μm	1.10 μm	0.48 μm

In closing, we should note that the formal errors given here are measures of only the internal consistency of our data, and do not yet imply accuracy of astrometric measurements at the 6 mas level. For example, we carefully chose the same set of stars each night to solve for the baseline vector of the interferometer; all of these stars had good hour-angle coverage. Using a different set of stars for baseline determination may have yielded positions more than 1σ away from the positions reported here. In addition, other potential sources of systematic error cannot be addressed with the limited dataset available here. In constructing a catalog, it will be necessary to perform a global solution using a much larger dataset including stars covering a large fraction of the sky. This more complex problem will not be addressed with interferometric data for several more years. However, the results reported here are quite encouraging for interferometric astrometry. A principal strength of our approach to interferometric astrometry is the combination of instrument development and modification based on observations and real data.

REFERENCES

Colavita, M. M, Shao, M., and Staelin, D. H. (1987). Appl. Opt. **26**, 4113.

Kaplan, G. H., Hughes, J. A., Seidelmann, P. K., Smith, C. A., and Yallop, B. D. (1989). Astron. J. **97**, 1197.

Mozurkewich, D., Hutter, D. J., Johnston, K. J., Simon, R. S., Shao, M., Colavita, M. M., Staelin, D. H., Hines, B. E., Hershey, J. L., Hughes, J. A., and Kaplan, G. H. (1988). Astron. J. **95**, 1269.

Pan, X. P., Shao, M., Colavita, M. M., Mozurkewich, D., Simon, R. S., and Johnston, K. J. (1990). Astrophys. J. **356**, 641.

Shao, M., Colavita, M. M., Hines, B. E., Staelin, D. H., Hutter, D. J., Johnston, K. J., Mozurkewich, D., Simon, R. S., Hershey, J. L., Hughes, J. A., and Kaplan, G. H. (1988). Astron. Astrophys. **193**, 357.